Critical Liquid-Vapor Interface in SF_6. I. Thickness of the Diffuse Transition Layer

E. S. Wu* and W. W. Webb

School of Applied and Engineering Physics, and Laboratory for Atomic and Solid State Physics, Cornell University, Ithaca, New York 14850

(Received 27 April 1973)

Below the critical point the liquid-vapor interface of a simple fluid is characterized by a thin transition layer across which the values of density vary between the two phases. This transition layer can be described by a density profile characterized by an effective interface thickness L. As the temperature T approaches the critical temperature T_c, L diverges as $\epsilon^{-\nu'}$, where $\epsilon = 1 - T/T_c$. From the measurement of optical reflectivity of the liquid-vapor interface of sulfur hexafluoride, we have deduced the interface thickness and the critical index β for the coexistence curve. In the temperature range $9.73 \times 10^{-5} \leq \epsilon \leq 5.33 \times 10^{-2}$ we find $\nu' = 0.620 \pm 0.01$ if an error-function profile is assumed as proposed by Buff, Lovett, and Stillinger, or $\nu' = 0.663 \pm 0.02$ if the density profile proposed by Fisk and Widom is used. For both profiles β is found equal to 0.333 ± 0.008. These indices, when combined with the critical index γ' for the isothermal compressiblity and μ for the surface tension, are used to test various scaling relations.

I. INTRODUCTION

Far below the critical point, the liquid and vapor phases of a simple fluid in a weak gravitational field are separated by a sharp interface. As the critical point is approached, this interface thickens and becomes diffuse, spreading into the bulk phases until, at the critical point, it fills the whole volume of the system. At this point two phases have merged into one homogeneous phase. van der Waals first gave a detailed theory of this diffuse interface in 1894.[1] Based on his famous equation of state, he showed that the interface thickness[2] L becomes infinite at the critical point. Cahn and Hilliard[3] extended the same idea to critical mixtures. According to their theories the density distribution across the simple fluid interface can be described by the function (henceforth designated TANH)

$$\rho(x) = \tfrac{1}{2}(\rho_l + \rho_v) + \tfrac{1}{2}(\rho_l - \rho_v)\tanh(2x/L), \tag{1}$$

where $\rho(x)$ is density at height x, and ρ_l and ρ_v are densities of the liquid and vapor phase, respectively. Fisk and Widom[4] generalized Cahn and Hilliard's approach by replacing the classical analytic behavior of the extended thermodynamic function near the critical point by a scaling hypothesis corresponding to extension of scaling laws for the one-phase region into intermediate densities. Assuming a simple equation of state, they obtained a density profile (henceforth designated as FWF);

$$\rho(x) = \tfrac{1}{2}(\rho_l + \rho_v) + \tfrac{1}{2}(\rho_l - \rho_v)\left(\frac{\sqrt{2}\tanh(\sqrt{6}\,x/L)}{[3 - \tanh^2(\sqrt{6}\,x/L)]^{1/2}}\right). \tag{2}$$

A different approach was suggested by Buff, Lovett, and Stillinger (BLS).[5] Based on excitations having the potential energy of capillary waves like those introduced by Mandelstam[6] as normal modes, they arrived at an error-function density profile (henceforth designated as ERF)

$$\rho(x) = \tfrac{1}{2}(\rho_l + \rho_v) + \tfrac{1}{2}(\rho_l - \rho_v)\,\mathrm{erf}(\sqrt{\pi}\,x/L). \tag{3}$$

This profile is remarkably similar to the profile provided by Fisk and Widom except at large x, where the FWF profile approaches an asymptotic exponential form $e^{-x/L'}$.[2] Here L' is the decay length. Relations between L and L' for various density profiles are given in Ref. 8.

Knowing the density profile, it is possible to compute the optical reflectivity as a function of interface thickness L and the square of the density difference $(\Delta\rho)^2$. Gilmer, Gilmore, Huang, and Webb[7] made the first measurements of the effective thickness of the interface by observing the reflectivity of the interface in binary mixtures of cyclohexane and methanol near the critical temperature. Assuming the hyperbolic tangent concentration distribution suggested by Cahn and Hilliard, and the critical divergence of L in the usual form $L = L_0(1 - T/T_c)^{-\nu'}$, where T_c is the critical temperature, they found that $\nu' = 0.76$ gave a best fit of their data, instead of $\nu' = 0.50$, as predicted by van der Waals and by mean-field theory. Later on, Huang and Webb[8] performed more accurate measurements on the same system, and included the FWF and ERF concentration distributions of the critical interface in their data fitting. They clearly excluded the hyperbolic tangent concentration profile and found that both the error-function profile of BLS and the Fisk-Widom profile fitted

their results satisfactorily within the experimental error. They also found that near the critical point, L diverges with a temperature exponent ν' equal to 0.67 ± 0.02.

The interface thickness has been related to the correlation lengths of the bulk phases by Fisk and Widom.[4,9,10] Based on the scaling and homogeneity arguments, Widom made the conjecture that, in whatever guise it might appear, there is only one length of fundamental significance in the critical phenomena. This would lead one to identify the interface thickness with the correlation length ξ' in either of the bulk phases. This conjecture has been tested in mixtures by the direct interface-thickness measurements of Huang and Webb. Their results on $\nu' = 0.67 \pm 0.02$ are in good agreement with the values calculated for ξ' from the data of Balta and Gravett.[11] Numerical analysis of the three-dimensional lattice-gas models yields $\nu = 0.643$ [12] and $\nu = 0.638$ [13] for the correlation length index above T_c; below T_c no direct calculation of ν' has been made, but Fisher[12] has estimated $\nu' = 0.675$ for the three-dimensional lattice gas in agreement with Huang and Webb's results. The theory of Fisk and Widom also yields a relation amongst the critical exponents ν', μ for the surface tension σ, β for the coexisting density difference $\Delta\rho$, and γ' for the isothermal compressibility K_T or its analog. Gilmer, Gilmore, Huang, and Webb also determined β and Warren and Webb[14] determined μ. However, the exponent γ' was missing and had to be guessed. The results suggested, but did not demonstrate, that two-parameter scaling should be adequate. A more detailed discussion of these ideas is given in Huang and Webb,[8] Warren and Webb[14] and in Huang's thesis.[15]

Measurements of L, along with σ, $\Delta\rho$, and K_T with their critical exponents, μ, β, and γ' for a simple fluid offer a complete picture of the critical interface in a simple fluid and a better test of the Fisk-Widom theory. One might also hope to test the relation $\xi' = L'$, especially noting that this equation, if confirmed, would establish the relatively easy reflectivity measurement as a means to study the critical behavior of ξ', a quantity that has proven to be rather elusive.

Using straightforward laser-optical techniques, we have studied the diffuse interface in a critical simple fluid, sulfurhexafluoride. Critical bulk properties of this particular fluid have previously been studied in detail,[16] but some of the results have been subject to controversy. The present work is aimed to help to resolve some of this controversy. We measured the optical reflectivity of the liquid-vapor interface of SF_6 with extreme precision at six light wavelengths chosen from those provided by Ar-Kr and He-Ne lasers. Our measurements covered the temperature range $9.73 \times 10^{-5} \leq 1 - T/T_c \leq 5.33 \times 10^{-2}$. By fitting the temperature dependence of the results, we obtained the effective thickness L and its critical exponent ν' in the range $9.73 \times 10^{-5} \leq 1 - T/T_c \leq 5.33 \times 10^{-3}$ and as a byproduct the representative exponent β of the coexistence curve over a wide temperature range.

Since the determination of interface thickness L from the reflectivity is strongly dependent on the assumed density profile, one might expect that analysis of reflectivity data for a range of light wavelengths would reveal the precise nature of the density profiles. Unfortunately, this is not quite true because the measured reflectivities are sensitive to the central part of the density profile only and because the convenient range of light wavelengths is rather small. In order to maximize the discrimination of various profiles, we have resorted to a meticulous analysis of the wavelength dependence of the reflectivity. In Sec. II the experimental setup and sample controls are described. In Sec. III we present the measured data and the detailed statistical analysis. Conclusions and discussions are given in Sec. IV, where we discuss various scaling relations and test the postulate that L' is identical to the long-range correlation length in the bulk phases.

Paper II describes our quasielastic light-scattering studies of the dynamics of thermal excitations of this interface in SF_6. Data on the static critical behavior found in this paper are combined there with the data on the dynamics of thermal excitations to show additional features of the critical interface and to test particular features of critical phenomena in SF_6.

II. EXPERIMENTAL SETUP AND PROCEDURES

The sample, instrumental grade SF_6 with purity 99.99% obtained from Air Products and Chemicals, Inc., is compressed into a carefully cleaned sample cell whose volume can be changed by moving an attached flexible metal bellows. The whole assembly is thermally controlled with an accuracy of better than 0.001 °C. When the sample is heated up toward T_c the interface will disappear at the top or the bottom of the cell, depending on whether the average density is greater or less than ρ_c, the critical density. The sample volume is adjusted by moving the metal bellows in or out to obtain the right filling density with which the meniscus disappears at the center of the sample cell when the critical temperature is reached. The recorded T_c in our cell of 45.530 °C is referred via a Beckmann thermometer calibrated against our National Bureau of Standards calibrated platinum thermo-

meter to the standard temperature scale. This value of T_c agrees with the values reported in various earlier experiments.[17,18] We have made periodic checks of T_c; no deviation from 45.530 °C has been found in a period of two years.

The sealed sample cell is constructed of a massive block of beryllium copper chosen for its high thermal conductivity and reasonable strength. This cylindrical cell is 4.375 in. high and 4.5 in. outer diameter. Two fused-quartz windows are sealed on both flat ends by indium O-rings. Between the two windows is the sample holder with a volume of about 45 cm^3. The sample is thermally controlled within better than 0.001 °C throughout the experiments, with the aid of a double thermostat with a proportional response temperature control. Details are given in the thesis of Wu.[19]

Owing to the sample's high surface tension and low viscosity, the slightest floor vibration excites waves on the interface that may cause the reflected laser beam to flutter out of alignment with a spatial filter that is used to eliminate the background scattered light. To reduce the vibration to a minimum, the whole sample assembly and optical components are located on a flat 3700-lb granite table supported by three air cylinders. An air servo system is attached to these cylinders to keep the table top within 0.001 in. of the preset position. The low natural frequency (1.4 Hz) of the system, plus the heavy weight of the table top, provides adequate insulation from external disturbances.

The sample is always held at a constant temperature long enough to ensure that thermal-equilibrium conditions are reached before performing the reflectivity measurements. We have compared the measured reflectivity after the sample has waited at a constant temperature for various times up to 80 h and found that after 4 h they agreed. Ordinarily 4 h easily sufficed, but near T_c waits of up to 12 h were used for safety. We compared measurements at a fixed temperature approached both from above and below, and we found that the data agreed over our entire range of measurement, leaving little doubt that the system is in an equilibrium state. To detect the possibility of local heating by the incident laser beam, we also compared the measurements made with the laser light shining on the sample for a few seconds up to a few hours; no disagreement was found. In our measurement of reflectivity as a function of temperature, the temperature settings were chosen in random order to avoid the possibility of introducing error due to the time-dependent changes becoming proportional to change of temperature.

In a period of two years, we made two complete independent sets of measurements on the same system with fully compatible results. In the first measurements, we worked over a temperature range $0.031 \leq T_c - T \leq 17$ °C using the red light with wavelength 6328 Å from a He-Ne laser as light source. In the second set of measurements the optical setup is almost identical to that of the first one, except that the light sources are five spectral lines (6471, 5145, 4880, 4727, and 4579 Å) from a Coherent Radiation model No. 52-B Ar-Kr mixed gas laser, and the measurements are performed in the temperature range $0.051 \leq T_c - T \leq 17$ °C.

A schematic diagram of the optical system is shown in Fig. 1. The laser light is first attenuated to ensure the linearity of PM (photomultiplier) response; the attenuated light, after passing through a spatial filter, is split into two beams. One of the beams falls on the phototube monitoring the laser intensity. The other beam shines onto the liquid-vapor interface at nearly perpendicular incidence. Specularly reflected light is picked up by a mirror above the sample; it then goes through another spatial filter to eliminate the background and stray light and is finally detected by the second phototube. The amplified signals from the PM's are recorded, and the ratio of these two signals gives the desired *relative* reflectivity. A digital voltmeter takes the ratio of the output from the two PM's to provide a direct readout of the reflectivity.

The light beam passes through several windows and the upper phase of the sample, all contributing to background scattering that is superimposed on the reflection from the interface. At low temperature (large ΔT) the reflected light is always strong enough to neglect the contribution of background scattering and dark current associated with

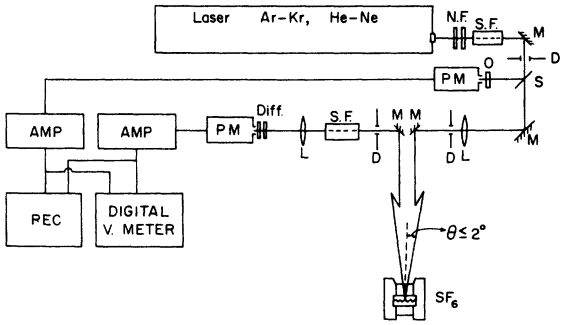

FIG. 1. Schematic diagram of the apparatus for reflectivity measurements. Lasers are Coherent Radiation 52B Ar-Kr mixed-gas laser and Spectra Physics 120 He-Ne laser, PM's are RCA IP21 photomultiplier; S.F. is spatial filter; M is mirror, L is achromatic lens; S is beam splitter; N.F. is neutral density filter; O. is opal diffuse glass; Diff. is diffuse glass plate; D is Iris diaphragm; AMP. is amplifier; and REC. is strip-chart recorder.

the PM, but as the temperature rises toward T_c the reflected intensity decreases sharply; therefore appropriate background corrections are necessary. For instance at $\Delta T = 1.0$ °C the background intensity is less than 1/1000 of the specular reflected intensity, but at $\Delta T = 0.1$ °C the background makes up 3.5% of the reflected intensity for violet light ($\lambda = 4579$ Å), and at the highest temperature $\Delta T = 0.051$ °C the background scattering makes up 75% of the detected light. This limits the accuracy of measurements close to T_c. For each wavelength the background intensity is nearly independent of temperature, suggesting that its source is residual scattering in the optical system rather than critical opalescence.

III. DATA ANALYSIS AND EXPERIMENTAL RESULTS

The interface separating the liquid and vapor phases consists of a thin transition layer across which densities vary from the value of liquid phase to that of vapor phase. This transition layer is characterized by a thickness L. If kL is much less than 2π, where k is the effective wave vector of the incident light, the optical reflectivity of a light shining normally onto this transition layer is[15]

$$R = \left(\frac{1}{n_l + n_v} \int_{-\infty}^{\infty} \frac{dn(x)}{dx} e^{-2ikx} \, dx \right)^2, \tag{4}$$

where $n(x)$ is the index of refraction at height x, and n_l and n_v are indices of refraction corresponding to liquid and vapor phases, respectively. The calculated reflectivities for TANH, FWF, and ERF density profiles are plotted in Fig. 2 as func-

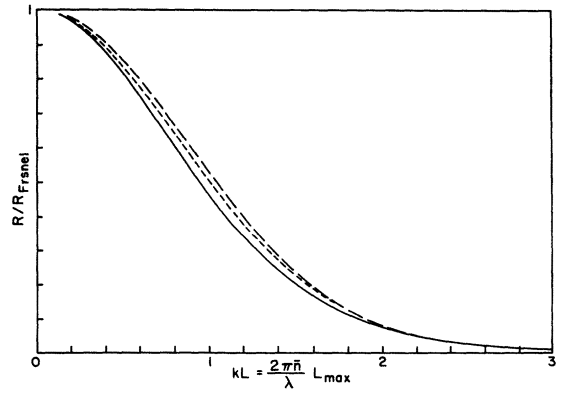

FIG. 2. Rayleigh-Gans approximation of the reflectivity ratio in normal incidence for the various distribution functions plotted as a function of kL, where the solid curve represents classical TANH function profile, short dashed curve represents FWF profile, and long dashed curve represents ERF profile.

TABLE I. Density profiles. $\rho(x)$ is the density at position x, the distance measured from the center of the density profile; ρ_l and ρ_v are liquid and vapor density, respectively. L is the effective interface thickness. $B(\Delta T)$ is a temperature-dependent constant; near the critical point $B(\Delta T) \propto (\Delta T)^{2\beta}$. $R(kL)$ is the reflectivity of normal incident light of wave vector k.

Function	Density profile	Reflectivity
Classical hyperbolic tangent function	$\rho(x) = \frac{1}{2}(\rho_l + \rho_v) + \frac{1}{2}(\rho_l - \rho_v)\tanh(2x/L)$	$R(kL) = B(\Delta T)\left(\frac{(\pi/2)kL}{\sinh(\pi/2)kL}\right)^2$
Error function	$\rho(x) = \frac{1}{2}(\rho_l + \rho_v) + \frac{1}{2}(\rho_l - \rho_v)\,\mathrm{erf}(\sqrt{\pi}\, x/L)$ $\mathrm{erf}(x) = \frac{2}{\sqrt{\pi}} \int_0^x e^{-t^2} \, dt$	$R(kL) = B(\Delta T) e^{(-2/\pi)k^2L^2}$
Fisk-Widom function	$\rho(x) = \frac{1}{2}(\rho_l + \rho_v) + \frac{1}{2}(\rho_l - \rho_v)\left(\frac{\sqrt{2}\tanh(\sqrt{6}\, x/L)}{[3 - \tanh^2(\sqrt{6}\, x/L)]^{1/2}}\right)$	$R(kL) = B(\Delta T)\left[\int_{-\infty}^{\infty} dx\, e^{-2ikLx} \frac{\mathrm{sech}^2\sqrt{6}\, x}{(1 - \frac{1}{8}\tanh^2\sqrt{6}\, x)^{3/2}}\right]^2$

tion of kL. Assuming the validity of the Lorentz-Lorenz equation near the critical point,[20] Eq. (4) can be rewritten as

$$R(kL) = C(\Delta T)^{2\beta}\left(\int_{-\infty}^{\infty}\frac{df(x)}{dx}e^{-2ikx}\,dx\right)^2, \qquad (5)$$

where $f(x)$ is the x-dependent part of the density profile $\rho(x)$, C is a proportional constant, and we have replaced $\Delta\rho$ by $\Delta\rho_0(\Delta T)^\beta$. As we can see from Eq. (5), a Fourier inversion would allow us to determine the quantity (df/dx), and if the density profile is antisymmetric with respect to origin, then the density profile can be determined. However this cannot be accomplished in practice because of the restricted range of available wavelengths. Therefore, instead of determining density profiles directly, we compute R for various hypothetical density profiles and compare with measured data. Table I defines the theoretical density profiles and their corresponding reflectivities.

We have made two independent sequences of reflectivity measurements. Only 6328Å light from a He-Ne laser was used in the first sequence over the temperature range $0.031\ ^\circ\text{C} \leq \Delta T \leq 17\ ^\circ\text{C}$ (or $9.73\times10^{-5} \leq \epsilon \leq 5.33\times10^{-2}$) where 121 evenly distributed data were taken. In our second sequence five different light wavelengths (4579, 4727, 4880, 5145, and 6471Å) from an Ar-Kr mixed gas laser were used as light sources. In Fig. 3 all of these reflectivities and the best-fit curves are plotted. The data from the two sequences are entirely consistent with each other. For convenience the second sequence is analyzed as a set and the first, which supplied only one intermediate wavelength, is treated as a consistency check.

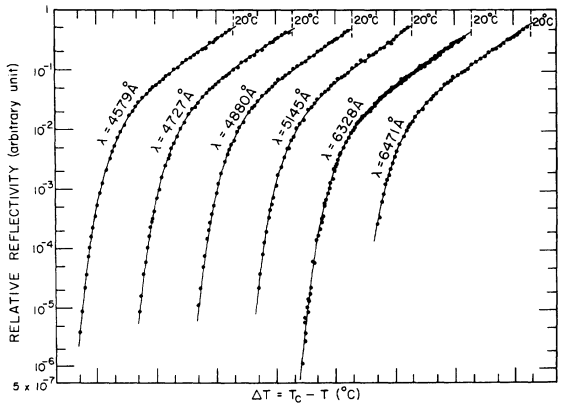

FIG. 3. Experimental reflectivity data for the normal incidence at six wavelengths. The reflectivity in arbitrary units is plotted against ΔT on a log-log scale. Solid lines are the best-fitted curve to the ERF. Note that the scales for ΔT are shifted for clarity.

Next the rather complex statistical analysis of the data is discussed. If interface thickness diverges with a single index ν',[21] i.e., $L = L_0(\Delta T/T_c)^{-\nu'}$, a numerical nonlinear least-squares fit will yield β, L_0, and ν' directly. Since the data points are evenly distributed in $\ln(R)$ to $\ln(\Delta T)$ scale, the best fitting variables are $\ln(R)$ instead of R. We are able to assume that the uncertainty in ΔT is negligible in our data range, so all the errors are associated with the measurement of R.

In our least-squares-fit procedure we minimize the quantity σ^2 defined in the following equation by varying the four parameters A, β, L_0, and ν':

$$\sigma^2 = N^{-1}\sum_{i=1}^{N}[\ln R_i - A - 2\beta\ln\epsilon_i - \ln F^2(kL_0\epsilon_i^{-\nu'})]^2, \qquad (6)$$

where R_i is the measured optical reflectivity at temperature, $\epsilon_i = 1 - T_i/T_c$, A is a constant, and $F(kL)$ is the quantity in the large parentheses of Eq. (5). There are five sets of these parameters corresponding to the values of five different wavelengths. These best fitted parameters are listed in Table II. We have tested the response of this fitting process to the change of each of the four parameters for all five wavelengths. The general features of the results of the fitting process are the same for each of the five wavelengths. Therefore the analyzed results for one arbitrarily chosen wavelength ($\lambda = 4880$ Å) are presented, although we have carried out the same analysis for all the wavelengths. The response of σ to the variation of one parameter from its best-fitted value, with all three other parameters assuming their best fitted values, is presented in Fig. 4. These curves indi-

TABLE II. Best-fit critical parameters. Critical parameters determined by the least-squares fit of reflectivity data to Eq. (6). β is the critical index for the coexistence curve. Parameters ν' and L_0 determine the interface thickness through the relation $L = L_0(T_c - T/T_c)^{-\nu'}$ Å. Effective wave vector $k = 2n\pi/\lambda$ is used in the fitting routine, where n is the index of refraction.

	λ	6471 Å	5145 Å	4880 Å	4727 Å	4579 Å	Average
ERF		0.325	0.331	0.331	0.334	0.335	0.332
FWF	β	0.330	0.334	0.332	0.334	0.332	0.333
TANH		0.336	0.353	0.356	0.361	0.364	0.352
ERF		0.6198	0.6286	0.6217	0.6094	0.6259	0.620
FWF	ν'	0.6775	0.6793	0.6654	0.6474	0.6556	0.663
TANH		0.7572	0.8211	0.8244	0.8252	0.8465	0.805
ERF		10.35	9.66	10.22	11.27	9.87	10.35
FWF	L_0 (Å)	6.37	6.46	7.94	8.45	7.96	7.37
TANH		3.14	1.94	1.91	1.86	1.62	2.19
ERF	$\langle\sigma^2\rangle^{1/2}$ $\times10^2$	3.260	4.844	3.182	3.216	3.411	3.583
FWF		3.353	4.951	3.290	3.394	3.793	3.748
TANH		3.701	5.729	4.381	4.638	5.275	5.494

cate that the least-squares fit is much more sensitive to the parameters L_0 and ν' than to the parameters A and β, or in other words, our data are more suitably used to determine L_0 and ν' than to determine A and β.

From Eq. (6) we can make a rough estimation of the standard deviations of parameters A and β. At large ΔT the quantity $\ln[F^2(kL)]$ in Eq. (6) can be neglected. Therefore in the large ΔT region it is reasonable to assume a linear relation between $\ln R_i$ and $\ln\epsilon_i$. Then the standard deviations σ_A^2 and σ_β^2 are given as

$$\sigma_A^2 = \sigma'^2 \sum_{i=1}^{N'} (\ln\epsilon_i)^2 \Big/ \Delta' \tag{7}$$

and

$$\sigma_\beta^2 = N'\sigma'^2/4\Delta' , \tag{8}$$

with

$$\sigma'^2 = \frac{1}{N'} \sum_{i=1}^{N'} (\ln R_i - A - 2\beta \ln\epsilon_i)^2$$

and

$$\Delta' = N' \sum_{i=1}^{N'} (\ln\epsilon_i)^2 - \left(\sum_{i=1}^{N'} \ln\epsilon_i \right)^2 .$$

Here N' represents the number of high ΔT data used in this rough estimate. Letting A and β assume their best fitted values and using the data in the temperature range $\Delta T \geq 2$ °C ($N' = 17$), we find $\sigma_A/A = 1.3\%$ and $\sigma_\beta/\beta = 2.7\%$. If we use the data in a different temperature range, we will find slightly different values for σ_A/A and σ_β/β, but these differences are small as compared to the error of this rough estimate. For instance, using the data in the temperature range $\Delta T \geq 1.0$ °C ($N' = 22$), the percentage errors of A and β are 1.27% and 3.04%, respectively. This further demonstrates that our data are not very sensitive to the variations of A and β.

Knowing the uncertainties of A and β, we can estimate the uncertainties of L and ν' due to the uncertainties in A and β. If we let A assume its best-fitted value and vary the values of β, then at each β a least-squares fit routinely yields a set of L_0 and ν'. Figure 5 shows the values of ν' and L_0 as a function of β for data of $\lambda = 4880$ Å and FWF density profile with A assuming its best-fitted value given in Table II. A similar plot of L_0 and ν' as a function of A, with β assuming its best-

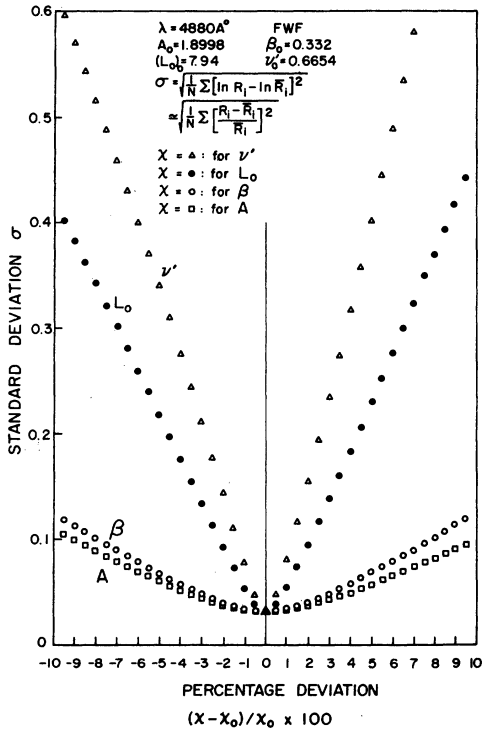

FIG. 4. Percentage change of standard deviation as each fitting parameter A, β, L_0, and ν' is varied individually around its best-fit value with all three other parameters fixed at their best-fit values. Data for 4880 Å with FWF profile; $A_0 = 1.8998$, $(L_0)_0 = 7.94$ Å, $\beta_0 = 0.332$, $\nu_0' = 0.6654$. The standard deviation $\sigma = [N^{-1}\sum(\ln R_i - \ln \bar{R}_i)^2]^{1/2} \simeq [N^{-1}\sum(R_i - \bar{R}_i/\bar{R}_i)^2]^{1/2}$. Data of other wavelengths show the same feature as this one.

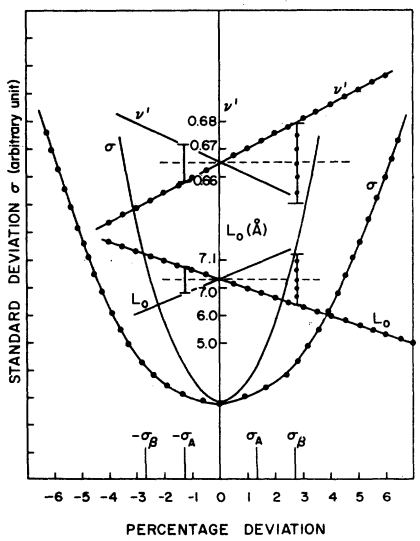

FIG. 5. Solid curves are the variations of ν' and L_0 as A deviates from its best-fitted value $A_0 = \ln 6.6849$ and with β assuming its best-fitted value $\beta_0 = 0.332$. Vertical bars are the uncertainties in ν' and L_0 due to the uncertainty in $A(\sigma_A)$. Curves with dots are the variations of ν' and L_0 as β deviates from β_0 with $A = A_0$. Vertical bars with dots are the uncertainties in ν' and L_0 due to the uncertainty in $\beta(\sigma_\beta)$. Data fit for 4880 Å with FWF density profile.

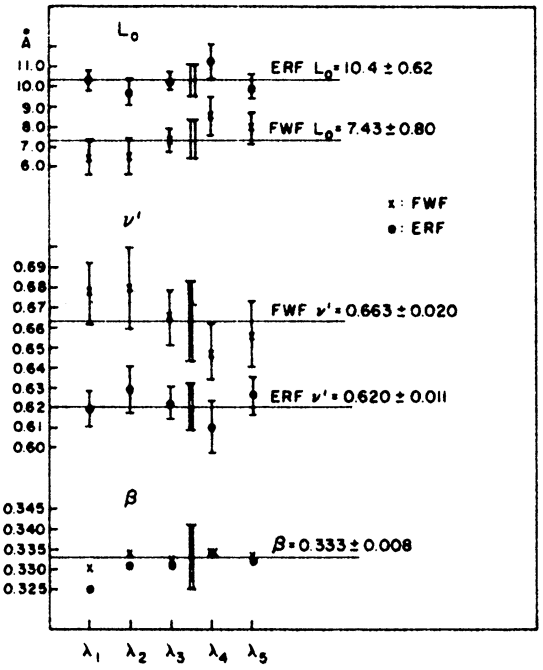

FIG. 6. Final values for parameters L_0, ν', and β at five wavelengths and two density profiles. Horizontal lines show the weighted average values. Double vertical bars show the uncertainties of averaged values. λ_1 = 6471 Å; λ_2 = 5145 Å; λ_3 = 4880 Å; λ_4 = 4727 Å; λ_5 = 4579 Å.

fitted value, is also shown in Fig. 5. In this figure the uncertainties in ν' and L_0 due to the uncertainties in A and β are shown as vertical bars. Since the statistical standard deviations for ν' and L_0 determined in the four-parameters-least-squares-fit process [Eq. (6)] are much smaller than the uncertainties due to the uncertainty in β, we chose the latter as the uncertainties for ν' and L_0. In this particular case, as shown in Fig. 5, the uncertainty in ν' is about 0.014 and the uncertainty in L_0 is about 0.9 Å.

We have performed the same analysis for the other wavelengths and for the ERF density profile. In Fig. 6 we have shown the parameters β, L_0, and ν' for all five wavelengths and the corresponding uncertainties estimated by the same approach that we used to obtain the uncertainties for the parameters of the λ = 4880 Å data. In Fig. 6 the horizontal lines are the weighted average values of five wavelengths with weighting factors equal to $1/\sigma^2$. The vertical double bars are the estimated uncertainties. The uncertainty for ν' is the sum of the following two uncertainties: (i) the standard deviation from their mean value

$$\sigma_1 = \left(\frac{1}{5} \sum_{i=1}^{5} [\nu'(\lambda_i) - \bar{\nu}']^2 \right)^{1/2} ,$$

where $\nu'(\lambda_i)$ is the ν' of wavelength λ_i and $\bar{\nu}'$ is the mean value defined as

$$\bar{\nu}' = \frac{1}{5} \sum_{i=1}^{5} \nu'(\lambda_i) ;$$

(ii) the standard deviations associated with each $\nu'(\lambda_i)$

$$\sigma_2 = \left[\sum_{i=1}^{5} \left(\frac{1}{\sigma_{\nu'(\lambda_i)}} \right)^2 \right]^{-1/2} ,$$

where $\sigma_{\nu'(\lambda_i)}$ is the standard deviation of $\nu'(\lambda_i)$. For the FWF density profile we find $\sigma_1 = 0.0125$ and $\sigma_2 = 0.0072$, so $\sigma_{\nu'} = 0.020$. For ERF we have $\sigma_1 = 0.0067$, $\sigma_2 = 0.0046$, and $\sigma_{\nu'} = 0.011$. The uncertainty for L_0 is estimated in the same way, and the results are listed in Table III.

Finally we want to know whether both L_0 and ν' can vary substantially together in such a way as to seem to yield a fairly small standard deviation. The answer to this question is no. We have fixed A and β at their best-fitted values and calculated the standard deviations σ as a function of both L_0 and ν'. Equal-σ contours show that the joint

TABLE III. Contribution of density-profile choice to estimated error. β is the critical index of the coexistence curve. L_0 and L_0' are the effective thickness and corresponding decay length at $(1 - T/T_c) = 1$. $\langle \sigma_L^2 \rangle^{1/2}$ is the standard error of estimate of L as calculated for each density profile without the assumption of a particular temperature dependence for L. $\langle \sigma_0 \rangle \sim 3\%$ is the estimated random error of measurement of L. The last column gives the excess error introduced by the assumption of each density profile.

Density profile	β	ν'	L_0 (Å)	L_0' (Å)	$\langle \sigma_L^2 \rangle^{1/2}$	$\frac{\langle \sigma_L^2 \rangle^{1/2} - \langle \sigma_0 \rangle}{\langle \sigma_0 \rangle}$
Error function	0.332 ± 0.008	0.620 ± 0.011	10.4 ± 0.62	···	3.21%	7%
Fisk-Widom function	0.333 ± 0.008	0.663 ± 0.02	7.43 ± 0.80	1.52 ± 0.16	3.87%	29%
Classical function	0.352 ± 0.015	0.799 ± 0.05	2.46 ± 0.92	0.62 ± 0.22	9.11%	204%

variations of L_0 and ν' from their best assumed values cause little more deviation than the single-parameter variations.

From the first row of Table II, we can clearly see that the index β is only weakly dependent on the choice of density profiles. This can be understood because the quantity $(\Delta T)^{2\beta}$ in Eq. (5) is directly proportional to the Fresnel reflectivity R_f which represents the reflectivity in the asymptotic region where the data are insensitive to the choice of density profiles.

On the other hand, the values of ν' and L_0 are strongly dependent on the choice of density profiles. Therefore, we can not find a single set of ν' and L_0 that will satisfy both ERF and FWF profiles simultaneously. However, we noticed that by choosing the ERF profile the variations of the values of ν' and L_0 over five wavelengths are substantially less than those obtained by choosing the FWF profile. These have been shown in Fig. 7. From the last row of Table II we find that for each wavelength the analysis based on the ERF profile has consistently smaller standard deviations than the other two profiles. The difference between the values of standard deviations of ERF and FWF is small, but the hyperbolic tangent function has a 50% larger standard deviation than the other two. Within the temperature range we covered, the ERF profile yields the better fit to our measurements. To support this conclusion, we go further to analyze the wavelength dependence of interface thickness.

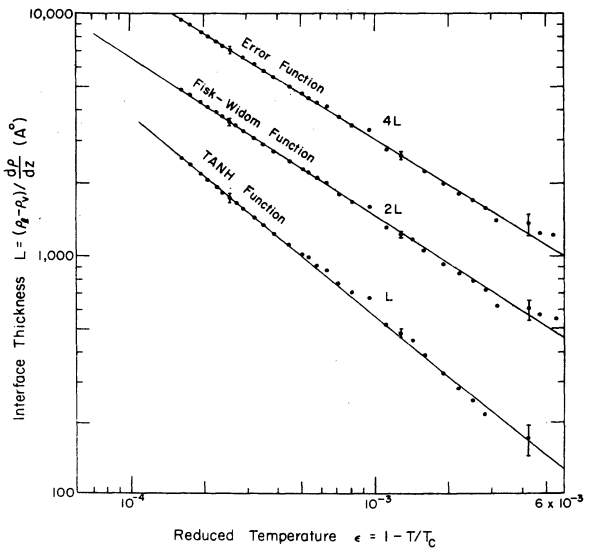

FIG. 7. Best effective thicknesses $L(T)$ obtained by fitting the second set of measurements for five wavelengths to ERF, FWF, and TANH density profiles. Solid lines represent the best-fitted power law $L = L_0\epsilon^{-\nu'}$. Each point represents the mean value over five wavelengths.

The interface thickness L for each measured R can be calculated with the parameters of Table II. At each temperature ΔT_i the average interface thickness $\bar{L}_i$ and the variance $\langle\sigma_i^2\rangle$ can be defined, respectively, as

$$\bar{L}_i = \tfrac{1}{5}\sum_{j=1}^{5} L_{ij}$$

and

$$\langle\sigma_i^2\rangle = \tfrac{1}{5}\sum_{j=1}^{5}\left(\frac{(L_{ij}-\bar{L}_i)}{\bar{L}_i}\right)^2 ,$$

where $L_{ij} = L(\Delta T_i, \lambda_j)$ is the interface thickness at temperature ΔT_i and wavelength λ_j. In the absence of error, the values of L_i at fixed temperature ΔT_i should be independent of λ_j for the correct density profiles. Therefore the quantity

$$\langle\sigma_L^2\rangle = \frac{1}{N}\sum_{i=1}^{N}\langle\sigma_i^2\rangle ,$$

which is the average standard fractional deviation of thickness L determined without the assumption of any particular temperature dependence for L, can be used to choose the best density profiles. In column 6 of Table III, we have listed calculated values of $\langle\sigma_L^2\rangle$ for various density profiles. A comparison of these values with the estimated random-measurement error (3%) for L shows that the ERF profile agrees with our data very well, while FWF and hyperbolic tangent-function profiles have excess deviations of 29% and 204%, respectively, as shown in the last column of Table III. These analyses further support the result we obtained in the last paragraph, that the ERF profile seems to fit our data best. However, we again recall that most of our data are sensitive to the central part of the density profiles only, while it is in the tails of those profiles that ERF and FWF differ most.

To determine the temperature dependence of the interface thickness, we have chosen $\bar{L}_i$ as the most likely value of L at ΔT_i and performed the least-squares fit of $\bar{L}_i$ and ΔT_i against the relation $L = L_0(\Delta T/T_c)^{-\nu'}$. The variance $\langle\sigma_i^2\rangle$ increases as does ΔT_i. This is because L is determined by $(R_f' - R)/R_f'$ instead of R; here R_f' is the relative Fresnel reflectivity, which differs from R_f by the same proportional factor as R differs from absolute reflectivity. To avoid this inessential variation we have chosen only the data below $\Delta T = 1.7$ °C for the determination of the temperature dependence of L. Instead of giving the same weight to every $\bar{L}_i$, we assign a weighting factor $\omega_i = 1/\langle\sigma_i^2\rangle$ for each $\bar{L}_i$. Furthermore, a fractional uncertainty, rather than a constant uncertainty in L, repre-

sents the measurement errors best. We therefore deduce the values of ν' and L_0 by performing the least-squares fit on a log-log scale rather than on a linear scale. We have performed the analysis at different temperature ranges, and values of ν' and L_0 for various density profiles are listed in Table IV. In ERF and FWF density profiles no systematic change in the values of ν' and L_0 are found. Their average values are in good agreement with the values listed in Table II. The final values for ν' and L_0 together with their estimated uncertainties are given in Table III. In Fig. 7 we have plotted the measured interface thickness of various density profiles, and Fig. 8 shows the combination of our two sets of independently measured L.

In the temperature range $0.051 \leq \Delta T \leq 17$ °C ($9.73\times10^{-5} \leq \epsilon \leq 5.33\times10^{-2}$), our best estimated value for β is 0.333 ± 0.008. This value is in good agreement with the values reported previously,[22-24] but there would be no reason to doubt, and much reason to believe, that β may assume slightly different values other than 0.333 as the measurement is getting closer to T_c, or eventually it may even approach a universal value, as is always being argued. With sufficient accuracy one might expect β to converge toward a value between 0.34 and 0.35 as $T \to T_c$, since $\beta = 0.35$ for CO_2[25] and $\beta = 0.35$ for Xe.[26] Therefore we chose a set of values ranging from 0.33 to 0.35 for β, instead of leaving it as a free adjustable parameter in the data-fitting process [Eq. (6)]. The least-squares fit results show that the fitting gets worse as β increases, just as we expect. In the extreme case when $\beta = 0.35$, the standard deviation increases as much as 50% over the best-fitted value. This is beyond the range that can be tolerated by our experimental errors.

In our data analysis we have assumed that β has a constant value throughout the whole temperature range. This assumption has previously been established by the coexistence-curve measurement of Benedek, Lastovka, Giglio, and Cannell[16] and of Tison and Hunt.[23] Recently, Balzarini and Ohrn[24] determined the coexistence curve of SF_6 by interferometric measurements. They found $\beta = 0.346 \pm 0.001$ in the range $10^{-2} \leq \epsilon \leq 10^{-1}$, and $\beta = 0.339 \pm 0.003$ in the range $\epsilon \leq 3\times10^{-3}$. Our value of β is determined by the least-squares-fit routine of Eq. (6). The single value of β thus obtained proved to be insensitive to the selected temperature range of the fitting process. Therefore from our data we would not expect to find the small change in β reported by Balzarini and Ohrn.[24] Our values of ν' and L_0 are determined by the data in the temperature range $9.73\times10^{-5} \leq \epsilon \leq 5.33\times10^{-3}$, and within the range $3\times10^{-3} \leq \epsilon \leq 5.33\times10^{-3}$ there are only a few lightly weighted data points, while all heavily weighted data points are in the temperature range $\epsilon \leq 3\times10^{-3}$; therefore we are confident that the extremely weak temperature dependence of β has little effect on our values of ν' and L_0. If we set $\beta = 0.339$, as determined in Ref. 24, we find $L = 9.08\epsilon^{-0.634}$ Å for ERF and $L = 6.55\epsilon^{-0.676}$ Å for FWF in comparison with our best values, $10.4\epsilon^{-0.620}$ and $7.43\epsilon^{-0.663}$, respectively.

TABLE IV. Temperature-range dependence of critical exponent ν'. Results of the least-squares fit of $\bar{L}_i$ against the relation $L = L_0(\Delta T/T_c)^{-\nu'}$ at different temperature ranges. A weighting factor $\omega_i = 1/\sigma_i^2$ is assigned to $\bar{L}_i$.

Data point	Temperature range	TANH L_0 (Å)	TANH ν'	ERF L_0 (Å)	ERF ν'	FWF L_0 (Å)	FWF ν'
33	$0.051 \leq \Delta T \leq 1.7$	2.74	0.7801	10.55	0.6181	7.68	0.6590
32	$0.051 \leq \Delta T \leq 1.5$	2.74	0.7798	10.48	0.6189	7.60	0.6602
31	$0.051 \leq \Delta T \leq 1.35$	2.75	0.7795	10.46	0.6191	7.38	0.6638
30	$0.051 \leq \Delta T \leq 1.15$	2.77	0.7785	10.34	0.6205	7.32	0.6648
29	$0.051 \leq \Delta T \leq 0.995$	2.77	0.7783	10.35	0.6204	7.33	0.6646
28	$0.051 \leq \Delta T \leq 0.897$	2.78	0.7781	10.37	0.6202	7.34	0.6645
27	$0.051 \leq \Delta T \leq 0.799$	2.84	0.7751	10.45	0.6193	7.35	0.6643
	Linear average	2.77	0.7785	10.43	0.6195	7.43	0.6630

IV. DISCUSSION

In order to extract the maximum information from our reflectivity measurements, we have carried out an elaborate five-parameter fit of the net

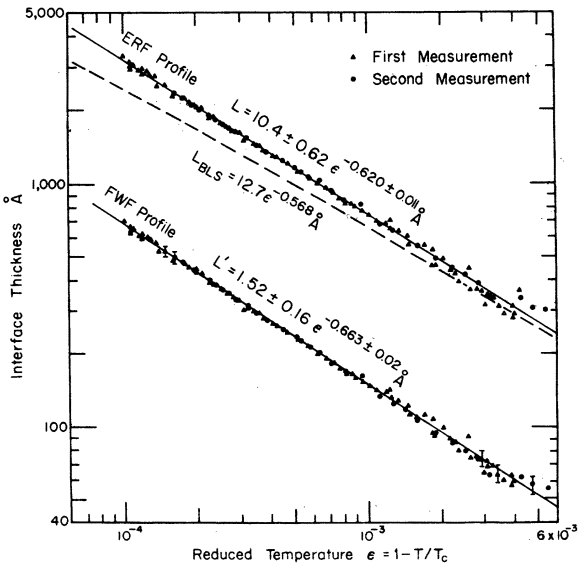

FIG. 8. Effective thickness L for the ERF and decay length L' for the FWF are plotted against reduced temperature on log-log scale with all of our data (first and second sets of measurements). Note that differently defined characteristic lengths are used. L' is the decay length that can be identified as the correlation length in the Fisk-Widom theory. Best-fitted power laws are displayed along respective curves.

of temperature- and wavelength-dependent reflectivities. Temperature dependence of each critical parameter is at first heuristically taken in the form $x = x_0\epsilon^{\chi}$, where x_0 and χ are taken to be constants in a selected temperature range. Based on relevant theories, we have selected three trial functions for the interface-density profiles and have fitted our reflectivity data using each independently. The same routine can be applied to other profiles that may be proposed. However, we have not found it practical to fit the data without a trial profile.

We find that both an error function and the Fisk-Widom function provide good representations of the interface-density profile in the temperature range $9.73\times10^{-5} \leq 1 - T/T_c \leq 5.33\times10^{-3}$, while the classical hyperbolic-tangent function does not. For both ERF and FWF, β is found to be 0.333 ± 0.008 in the temperature range $9.73\times10^{-5} \leq 1 - T/T_c \leq 5.33\times10^{-2}$; this value is in good agreement with previously reported values. The interface thickness determined using the ERF profile is

$$L = (10.4 \pm 0.62)\epsilon^{-0.620 \pm 0.01}\ \text{Å}, \tag{9}$$

and within the estimated uncertainty, this result is just barely consistent with the value of L obtained by using FWF,

$$L = (7.43 \pm 0.80)\epsilon^{-0.663 \pm 0.02}\ \text{Å}, \tag{10}$$

where $L = 2\sqrt{6}\,L'$ and the decay length L' is

$$L' = (1.52 \pm 0.16)\epsilon^{-0.663 \pm 0.02}\ \text{Å}.$$

Our data analysis showed that the ERF density profile fits our measurements slightly better than FWF. Since the error-function profile does not have an exponential-decay tail, no exponential-decay length is defined for ERF. However in the range of our data, we can conjecture that the interface thickness determined by the error-function profile has the same sort of singular behavior as does the range of correlation ξ. Therefore the interface-thickness divergence (as $\epsilon^{-\nu'}$) may require $\nu' = 0.62 \pm 0.01$, as determined with ERF, instead of as $\nu' = 0.66 \pm 0.02$, as determined with FWF. Somewhere between is probably the best choice.

Fisk and Widom indicate that L' can be identified as the correlation length ξ' below T_c. In order to test the relation $L' = \xi'$ we must know the correlation length below T_c. Unfortunately, the only available data are measured along the critical isochore. From the measurement of total scattering power above T_c, Puglielli and Ford[27] found

$$\xi = 1.5 \pm 0.23(-\epsilon)^{-0.67 \pm 0.07}\ \text{Å}. \tag{11}$$

A recent study of Rayleigh linewidth[28] has yielded the singular part of thermal diffusivity. After inserting in Kawasaki's relation for thermal diffusivity in the hydrodynamic region our recently obtained[29] correct value of viscosity, the correlation length can be expressed as

$$\xi = 2.0 \pm 0.3(-\epsilon)^{-0.61 \pm 0.04}\ \text{Å}. \tag{12}$$

Both ξ_0 have fairly large uncertainties; nevertheless, if we let $\xi_0' = L_0'$, as suggested by Widom's theory, neither of them satisfies the condition $\xi_0/\xi_0' \sim 2$, suggested by the two-dimensional lattice-gas model.[12] No independent estimation of the ratio ξ_0/ξ_0' in three-dimensional Ising models has yet been made, but it is reasonable to guess that its value lies between the mean-field value $\sqrt{2}$ and the two-dimensional Ising-model value of 2. Therefore, a likely value is $\xi_0/\xi_0' \sim 1.6$,[30] as for the three-dimensional Ising models. This value barely agrees with $\xi_0/\xi_0' = 1.32 \pm 0.24$, obtained by using the revised Rayleigh-linewidth value $\xi_0 = 2.0 \pm 0.3$ of Eq. (12) above T_c and by assuming $\xi_0' = L_0'$ below T_c. The Rayleigh-linewidth data are discussed further in Paper II.[29] Fisher[30] has deduced a universal rule for estimation of the scale of the correlation-length variation near the critical point from the behavior of the Ising model. With the correlation length given by $\xi' = \xi_0'\epsilon^{-\nu'}$, the scale is determined by ξ_0', which he supposed to be closely related to the lattice spacing in the Ising model. Extending his idea to a critical simple fluid, he suggested that, below T_c, $\xi_0' \simeq 0.3(\rho_c)^{-1/3}$, ρ_c being the particle density at T_c. For SF_6 this implies $\xi_0' \sim 2.05$ Å.

With $\gamma = 1.235 \pm 0.015$,[28] and assuming $\nu = \nu' = 0.663$, we find that the value of index $\eta = 2 - \gamma/\nu$ introduced by Fisher[31] to account for the deviation of ξ' (or L' here) from the Ornstein-Zernike theory as $T \to T_c$ is $\eta = 2 - \gamma/\nu = 0.137 \pm 0.06$. On the other hand, with the ERF value of ν we have the opposite extreme, $\eta = 0.01$. The first value is a little bit larger than the three-dimensional lattice-gas prediction that $\eta = 0.056 \pm 0.008$[12] and $\eta = 0.074 \pm 0.035$[32] for CO_2, and that $\eta = 0.065$[33] for Xe, but is not unreasonable. The second value is consistent with two-parameter scaling. Clearly, our determination of η is lost in the small uncertainty in determination of ν' (0.62 vs 0.66) that arises from the choice of interface.

Finally, we must discuss the FWF and ERF density profiles that have been used in our data analysis. We have determined the optical reflectivity with better accuracy than has been achieved in previous experiments,[8] and we are able to see the small difference between these two functions in the k dependence of R/R_f. We find that ERF provides consistently better fit to our measurements than does FWF, and in fact must be very close to the exact function, at least in the central

portion of the interface. The ERF density profile assumes the form $\exp(-\pi z^2/L^2)$ in the asymptotic region, while it is usually expected that the functional form of the density profile has exponential tails.[4] The reflectivity is, however, insensitive to the shape of the tails.

The BLS theory describes the interface in terms of the second moment $\langle L_{\rm BLS}^2\rangle$ of the normalized density gradient; our $L=(2\pi\langle L_{\rm BLS}^2\rangle)^{1/2}$ for the ERF profile. BLS theory gives $L_{\rm BLS}$ in terms of the surface tension σ and density difference as

$$L_{\rm BLS}^2=(k_B T/2\sigma^0)\ln[1+(\sigma^0/\Delta\rho g)(\pi^2/L_{\rm BLS}^2)]\ , \quad (13)$$

where $\sigma^0=\sigma+(3k_B T/16)\pi^2/L_{\rm BLS}^2$. Using our surface-tension values from Paper II and published values of $\Delta\rho$,[16] we have estimated the interface thickness $L_{\rm BLS}$ predicted by the BLS theory. The results are shown as a dashed line in Fig. 8. In the temperature range we covered, a straight-line fit to this curve is reasonably satisfactory and yields the relation $L_{\rm BLS}=12.7\epsilon^{-0.568}$ Å, which can be compared with the best fit to the data $L=10.4\epsilon^{-0.62}$ Å. Although the BLS result is in qualitative agreement with our experiments, the systematic deviations are obvious and clearly exceed the experimental uncertainties.

Huang[34] had shown that the intensity and angular distribution of the light scattering by the interface are inconsistent with the model used by Buff, Lovett, and Stillinger to deduce the error-function profile. Their capillary-wave model allows a spectrum of only small k sharp-boundary wave-like modes along the plane of the interface. They are supposed to superimpose to form the diffuse boundary. However, the light scattering by these modes appears at such small angles around the specular reflection that the scattered light would be included in Huang's measurements of the specular reflection. Therefore no decrease of the *measured* reflectivity would be expected in the BLS model. Huang has, on the other hand, measured the angular distribution of the scattered intensity from the interface in critical mixtures, which he finds to be in excellent agreement with that calculated for wavelike collective thermal excitations of the entire diffuse interface.

Consequently, it seems preferable to visualize the diffuse interface as a superposition of fluctuations on the scale of $\sim\xi'$ $\sim L'$ in all directions, as in the bulk fluid, that superimpose in the interface to form a transition region of thickness L'. The important thermal excitations of this interface are collective excitations of the entire interface that produce small surface wavelike elevations and depressions of the interface height that vary on a horizontal scale that is much larger than the thickness of the diffuse layer. This contradiction of the BLS theory weakened the basis for our choice of ERF as a trial function. However Buff has recently informed us that Lovett, DeHaven, Vieceli, and Buff[35] have developed a new generalized theory of the interface that yields an error-function-like profile without involving the wave model.

We have used the FWF profile in spite of its less-perfect fit to our data in order to compare the effective interface thickness with the bulk correlation length. The FWF density profile is obtained by assuming *ad hoc* a simple equation of state for the fluid system. Hence there is the possibility that the correct equation of state will yield a density profile that correctly represents the interface and provides a better fit to our data. On the other hand, the theory of Fisk and Widom explicitly assumes that the equation of state of the uniform fluids can be continued into densities within the two-phase region, and it may be possible that difficulties arise due to failure of that assumption. Further discussion of FWF and the Fisk-Widom theory follow in Paper II, where our measurements of the interfacial energy permit a more stringent analysis.

ACKNOWLEDGMENTS

This research was supported by the National Science Foundation and the Advanced Research Projects Agency through the Materials Science Center at Cornell. We are pleased to acknowledge helpful discussions with M. E. Fisher, B. Widom, G. Mulholland, and F. P. Buff.

---

* Present address: Department of Chemistry, Syracuse University, Syracuse, N.Y.

[1] J. D. van der Waals, Z. Phys. Chem. 13, 657 (1894).

[2] A detailed discussion of various definitions for interface thickness is given in Ref. 8. Here we follow the notation of Huang and Webb. L is the effective thickness of the maximum density gradient, L' is the decay length representing the exponential wings of the density profiles. In Widom's theory L' can be identified to correlation length ξ'.

[3] J. W. Cahn and J. E. Hilliard, J. Chem. Phys. 28, 258 (1958).

[4] S. Fisk and B. Widom, J. Chem. Phys. 50, 3219 (1969).

[5] F. P. Buff, R. A. Lovett, and F. H. Stillinger, Jr., Phys. Rev. Lett. 15, 621 (1965).

[6] L. I. Mandelstam, Ann. Phys. (Leipzig) 41, 609 (1913).

[7] G. H. Gilmer, W. Gilmore, J. S. Huang, and W. W. Webb, Phys. Rev. Lett. 14, 491 (1965).

[8]J. S. Huang and W. W. Webb, Bull Am. Phys. Soc. 12, 333 (1967); J. S. Huang and W. W. Webb, J. Chem. Phys. 50, 3677 (1969).
[9]B. Widom, J. Chem. Phys. 43, 3892 (1965).
[10]B. Widom, in *Phase Transitions and Critical Phenomena,* edited by C. Domb and M. S. Green (Academic, New York, 1972).
[11]Y. Balta and C. C. Gravett, J. Chem. Phys. 48, 3839 (1968).
[12]M. E. Fisher, Rept. Prog. Phys. 30, 615 (1967); M. E. Fisher and R. J. Burford, Phys. Rev. 156, 583 (1967).
[13]M. A. Moore, D. Jasnow and M. Wortis, Phys. Rev. Lett. 22, 940 (1969).
[14]C. Warren and W. W. Webb, J. Chem. Phys. 50, 3694 (1969).
[15]J. S. Huang, Ph.D. thesis, (Cornell University, 1969) (unpublished).
[16]G. B. Benedek, J. B. Lastovka, M. Giglio, and D. Cannell, in *Critical Phenomena,* edited by R. E. Mills and R. I. Jaffee (McGraw-Hill, New York, 1971).
[17]M. A. Weinberger and W. G. Schneider, Can. J. Chem. 30, 422 (1952).
[18]R. H. Wentorf, J. Chem. Phys. 24, 607 (1956).
[19]E. S. Wu, Ph.D. thesis (Cornell University, 1973) (unpublished).
[20]S. V. Larsen, R. D. Mountain, and R. Zwanzig, J. Chem. Phys. 42, 2187 (1965).
[21]Buff, Lovett, and Stillinger have suggested a different form for L, but in our temperature range their theory is indistinguishable from such a simple power law.
[22]L. A. Makarevich and E. S. Sokolova, Zh. Eksp. Teor. Fiz. Pis'ma Red. 4, 409 (1966) [JETP Lett. 4, 276 (1966)].
[23]J. K. Tison and E. R. Hunt, J. Chem. Phys. 54, 1526 (1971).
[24]D. Balzarini and K. Ohrn, Phys. Rev. Lett. 29, 840 (1972).
[25]A. Michels, B. Blaisse, and C. Michels, Proc. R. Soc. (Lond.) A 160, 358 (1937).
[26]H. W. Habgood and W. G. Schneider, Can. J. Chem. 32, 98 (1954); M. A. Weinberger and W. G. Schneider, Can. J. Chem. 30, 422 (1952).
[27]V. G. Puglielli and N. C. Ford, Jr., Phys. Rev. Lett. 25, 143 (1969).
[28]T. K. Lim, H. L. Swinney, K. H. Langley, and T. A. Kachnowski, Phys. Rev. Lett. 27, 1176 (1971).
[29]E. S. Wu and W. W. Webb, following paper, Phys. Rev. A 8, 2077 (1973), referred to as Paper II.
[30]M. E. Fisher, Proceedings of the Conference on Fluctuations in Superconductors (Stanford Research Institute, Menlo Park, Ca. 1968) (unpublished).
[31]M. E. Fisher, J. Math. Phys. 5, 944 (1964).
[32]J. H. Lunacek and D. S. Cannell, Phys. Rev. Lett. 27, 841 (1971).
[33]H. L. Swinney, D. L. Henry, and H. Z. Cummins, J. Phys. 33, C*l* -81 (1972); $\eta = 0.10 \pm 0.04$ is obtained from the relation $(3\gamma')/(2\beta+\gamma') = 2 - \eta$ by Smith, Giglio, and Benedek, Phys. Rev. Lett. 27, 1556 (1971).
[34]J. S. Huang and W. W. Webb (private communication).
[35]R. Lovett, P. W. DeHaven, J. J. Vieceli, Jr., and F. P. Buff, J. Chem. Phys. 58, 1880 (1973).